Dynamic Modeling of Antimicrobial Pore Formation in Engineered Tethered Membranes

William Hoiles and Vikram Krishnamurthy, *Fellow, IEEE*

***Abstract*—In this paper, a mesoscopic-to-observable dynamic model of the pore formation measurement platform is presented. The platform is composed of a controllable engineered tethered membrane. Using the mesoscopic-to-observable model and experimental measurements allows the platform to be used to gain insight into the pore formation dynamics of peptides in biological membranes. These results are useful for the development of novel drugs, gene delivery therapies, and controlling pore formation in cell-like bioreactors. The model consists of coarse-grained molecular dynamics, a continuum model composed of a generalized version of Fick's law of diffusion coupled with surface reaction–diffusion equations, and a fractional order macroscopic model. We consider the pore formation dynamics of the antimicrobial peptide PGLa using the dynamic model and experimental measurements from the platform. The results provide a possible reaction-mechanism for PGLa pore formation in charged and uncharged membranes, which accounts for binding, translocation, and oligomerization of PGLa. The reaction-mechanism suggests that PGLa not only increases the number of pores in negatively charged membranes, but also increases the lifetime of pores compared to PGLa pores in uncharged membranes. Though results for PGLa are presented, the dynamics model and platform can be used to investigate the pore formation dynamics of other peptides.**

***Index Terms*—Tethered bilayer lipid membrane, bioelectronic interface, generalized reaction-diffusion, coarse-grained molecular dynamics, fractional order operators.**

I. Introduction

PORE forming peptides are crucial to the attack and defense mechanisms of biological organisms. Understanding the chemical kinetics of pore forming peptides provides vital information of use to pharmacologists to target specific classes of peptides for in depth pharmaceutical screening for novel drugs. In this paper a dynamic models of the pore formation measurement platform (PFMP) is presented which can be used to gain insight into the pore formation reaction mechanism and potency of pore forming antimicrobial peptides. We apply the dynamic model and experimental measurements from the PFMP to study the pore formation dynamics of PGLa (*peptidyl-glycineleucine-carboxyamide*), a membrane-active antimicrobial peptide produced in specialized neuroepithelial cells in the African frog *Xenopus laevis* [1]. In addition to the antimicrobial activity of PGLa, it also contains anticancer [2], [3], antiviral [4], and antifungal properties [5]. The remarkable feature of PGLa is that it provides a potential source for new antibiotics against increasingly common multiresistant pathogens (i.e. "superbugs") such as *methicillin-resistant Staphylococcus aureus* [6].

A schematic of the PFMP is provided in Fig. 1. The mechanism of action of antimicrobial peptides involves the molecule binding to the membrane surface, then undergoing orientational, conformational, and oligomerization processes to create a conducting pore. The principle detection mechanism of the PFMP is that by measuring the current response of the PFMP it is possible to estimate the time dependent conductance of the tethered membrane using a dynamic model. The membrane conductance is dependent on the number of conducting pores in the tethered membrane. The tethered membrane surface is engineered to mimic prokaryotic, eukaryotic, and archaebacterial membranes, and can therefore be used to measure the specificity of attack of pore forming peptides. The benefit of using the PFMP compared to methods such as lytic experiments, gel electrophoresis, site-directed mutagensis, and cryoelectron microscopy [7]–[10] is that the tethering density, electrolyte composition, membrane composition, and applied transmembrane potential can all be controlled by the experimentalist. To gain insight into the reaction pathway leading to pore formation requires a dynamic model that accounts for the diffusion of the peptides in solution, and the reaction-diffusion processes present on the membrane surface.

The dynamic model is composed of three levels of abstraction: a fractional order macroscopic model, a generalized reaction-diffusion continuum model, and coarse-grained molecular dynamics (CGMD) as illustrated in Fig. 2. The macroscopic model accounts for diffusion limited process at the electrode surface and predicts the membrane conductance $G_m(t)$ given the measured current response $I(t)$ from the PFMP. The CGMD model is used to estimate the diffusion coefficient D of surface bound and transmembrane bound peptides, and is also used to gain insight into the dynamics of binding, translocation, and oligomerization required for pore formation. The computed diffusion coefficients are then used in a generalized reaction-diffusion model which accounts for the steric effects of molecules using a "Langmuir" like activity coefficient [12]. The generalized reaction-diffusion equation is coupled to the surface reaction equations via a "Langmuir-Hinshelwood" like equation classically used to describe surface binding of molecules. As conducting pores form in the tethered membrane, the conductance of the membrane will increase proportionally to the number of pores. This allows the concentration of surface bound pores to be used to estimate the membrane conductance $\hat{G}_m(t)$. Validation of a proposed pore formation reaction

Manuscript received May 27, 2015; revised September 14, 2015; accepted November 6, 2015. Date of publication March 2, 2016; date of current version April 5, 2016. The associate editor coordinating the review of this paper and approving it for publication was T. Nakano.

The authors are with the Department of Electrical and Computer Engineering, University of British Columbia, Vancouver V6T 1Z4, Canada (e-mail: whoiles@ece.ubc.ca; vikramk@ece.ubc.ca).

Digital Object Identifier 10.1109/TMBMC.2016.2537299

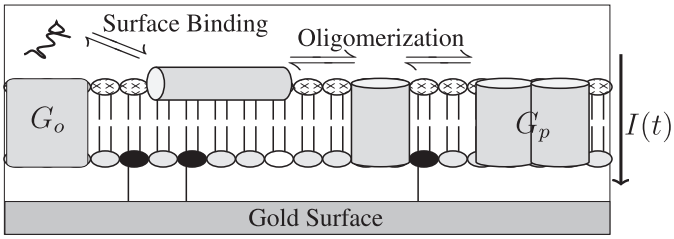

Fig. 1. Schematic of the Pore Formation Measurement Platform (PFMP). A voltage potential is applied between the gold electrode and counter electrode (not shown) and the current response $I(t)$ is measured. The PGLa peptide binds to the membrane surface, then undergoes oligomerization steps to create a PGLa pore with conductance G_p. The current response $I(t)$ of the PFMP is dependent on the number of conducing PGLa pores and the equilibrium number of aqueous pores with conductance G_o present in the tethered membrane. The dashed beads represent mobile lipids on the membrane surface, the gray beads are mobile lipids adjacent to the gold electrode, and the black beads are tethered lipids. The construction and formation of the PFMP is provided in [11].

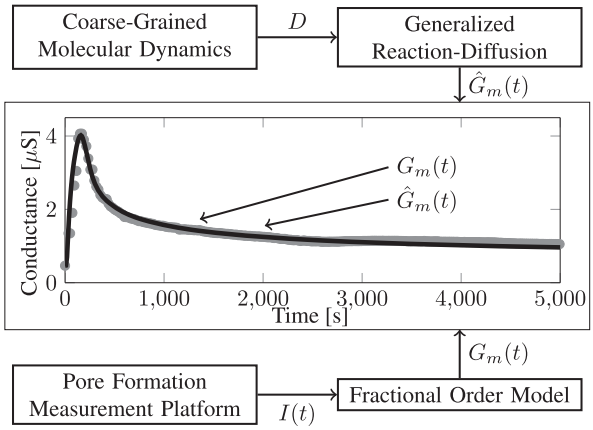

Fig. 2. Schematic of the mesoscopic-to-observable model. D is the diffusion coefficient of bound PGLa peptides, $\hat{G}_m(t)$ is the predicted conductance, $I(t)$ is the measured current from the PFMP (Fig. 1), and $G_m(t)$ is the measured conductance.

mechanism is achieved when the experimentally measured conductance $G_m(t)$ and numerically computed conductance $\hat{G}_m(t)$ are in agreement.

The paper proceeds by presenting the mesoscopic-to-observable dynamic model (Fig. 2) in Sec. II for the PFMP. In Sec. III numerical predictions of the pore formation dynamics of the antimicrobial peptide PGLa in a DphPC membrane are provided. DphPC archaebacterial lipids were selected for two primary reasons. First, DphPC lipids have been used extensively in the study of the interaction of proteins and peptides with membranes–especially in experiments in channel forming proteins (refer to [13]–[15] for details) as they are highly resistant to the permeability of ions. Second, using the DphPC lipids in the PFMP allows the membrane in the platform to remain intact for long periods of time (up to weeks) which make it ideal for studying the pore formation dynamics of PGLa. Sec. IV provides experimental measurements of the PFMP to exemplify the detection ability and model accuracy of the PFMP. Closing remarks are provided in Sec. V.

II. Dynamic Model

To estimate important biological parameters (e.g. membrane capacitance C_m and conductance $G_m(t)$) from the experimentally measured current response of the PFMP requires a dynamics model. In this section a mesoscopic-to-observable model is presented for the PFMP. The dynamic model is illustrated in Fig. 2 and is composed of three levels of abstraction: coarse-grained molecular dynamics, a generalized reactiond-diffusion equation, and a fractional order macroscopic model.

A. Fractional Order Macroscopic Model

In this section a fractional order macroscopic model is provided to compute the current response of the PFMP. The detection mechanism of PFMP is based on how the conductance of the tethered membrane increases as pores form in the membrane. The change in conductance is a measure of the potency of peptides on the membrane and can be used to estimate the reaction mechanism leading to pore formation. Fractional order operators are utilized in the model as the gold surface bioelectronic interface of the PFMP may contain diffusion-limited charge transfer, quasireversible charge transfer, and ionic adsorption dynamics. These double-layer charging effects can be modeled using fractional order operators [16].

The PFMP is composed of three distinct regions: the bioelectronic interface at the gold electrodes, the tethered membrane, and the bulk electrolyte solution. The membrane is assumed to be polarizable and to also contain aqueous pores as a result of random thermal fluctuations. This allows the tethered membrane to be modeled by an effective permittivity with capacitance C_m in parallel with the tethered membrane conductance $G_m(t)$ [11], [17], [18]. $G_m(t)$ is dependent on the population of aqueous pores and conducting PGLa pores present. Note that for membrane potentials below 50 mV, the population of aqueous pores is constant–that is, only the formation and destruction of PGLa pores will cause a change in the membrane conductance. Since a voltage excitation of 20 mV is used, the population of aqueous pores is constant and is accounted for by the associated equilibrium membrane conductance G_o. Therefore, any change in $G_m(t)$ is a result of PGLa pore formation. The bulk electrolyte solution is assumed to be purely ohmic with a resistance R_e. There exists an electrical double layer [19] at the bioelectronic interface of the PFMP which can be modeled using a capacitor if diffusion-limited charge transfer, quasireversible charge transfer, and ionic adsorption dynamics are not present. If these double-layer charging effects are present then the bioelectronic interface can be modeled using a constant-phase-element composed of a capacitance C_{dl} and the fractional order operator p. If $p < 1$ then a diffusion-limited process is present, and if $p = 1$ then a diffusion-limited process is not present. The electrode capacitance adjacent to the tethered membrane is denoted by C_{edl}, and the counter electrode capacitance by C_{cdl}. An excitation potential $V_s(t)$ is applied across the two electrodes of the PFMP and the current response $I(t)$ is measured. The fractional

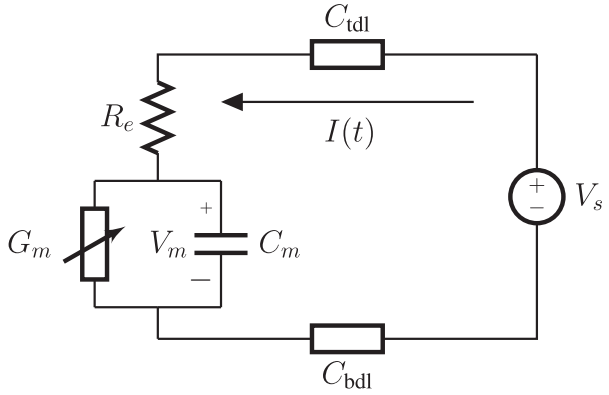

Fig. 3. Fractional order macroscopic model of the PFMP. The circuit parameters are defined in Sec. II-A.

order macroscopic model of the PFMP biosensor is given by (Fig. 3):

$$\frac{dV_m}{dt} = -\left(\frac{1}{C_m R_e} + \frac{G_m}{C_m}\right)V_m - \frac{1}{C_m R_e}V_{dl} + \frac{1}{C_m R_e}V_s,$$
$$\frac{d^p V_{dl}}{dt^p} = -\frac{1}{C_{dl} R_e}V_m - \frac{1}{C_{dl} R_e}V_{dl} + \frac{1}{C_{dl} R_e}V_s, \quad (1)$$
$$I(t) = \frac{1}{R_e}\left(V_s - V_m - V_{dl}\right), \quad (2)$$

where C_{dl} is the total capacitance of the gold electrode C_{edl} and counter gold electrode C_{cdl} in series with p in (1) the fractional order operator, V_m is the transmembrane potential, and V_{dl} is the double-layer potential. Given the drive potential $V_s(t)$, and the static circuit parameters C_{tdl}, C_{bdl}, C_m, and R_e, the membrane conductance $G_m(t)$ can be estimated from the measured current $I(t)$.

Using a sinusoidal drive potential $V_s(t) = V_o \sin(2\pi f t)$ with frequency f and magnitude V_o below 50 mV, the current response of the PFMP can be computed using a set of algebraic equations. Converting (1) and (2) into the complex domain with $V_s(t) = V_o \sin(2\pi f t)$, the current response of the PFMP is given by:

$$I(f) = V_o\left[R_e + \frac{1}{G_m + j2\pi f C_m} + \frac{1}{(j2\pi f)^p C_{dl}}\right]^{-1}. \quad (3)$$

In (3), j denotes the complex number $\sqrt{-1}$. Note that the impedance $Z(f)$ of the PFMP biosensor is given by the expression in $[\cdot]$ of (3). Assuming $G_m(t)$ is static during the measurement of $I(f)$, the membrane conductance $G_m(t)$ can be computed using a least-squares estimator with a cost function given by the difference between the measured current and the computed current from (3).

B. Generalized Reaction-Diffusion Model

In this section a generalized reaction-diffusion continuum model is presented to predict the dynamics of the membrane conductance for a given pore formation reaction mechanism. The reaction mechanism is validated when agreement between the experimentally measured conductance $G_m(t)$ from the fractional order model and the predicted membrane conductance $\hat{G}_m(t)$ is realized, refer to Fig. 2. The computational domain of the continuum model is provided in Fig. 4. A two-dimensional simulation domain is considered as the chamber width of the PFMP is $W = 3\,\text{mm}$ and chamber height $h_e = 0.1\,\text{mm}$. As shown in [20], for $h_e/W < 0.1$ the variation in concentration along the width of the chamber is negligible. For the PFMP the aspect ratio is $h_e/W = 0.03$, therefore a two-dimensional domain can be used to model the reaction-diffusion dynamics in the PFMP.

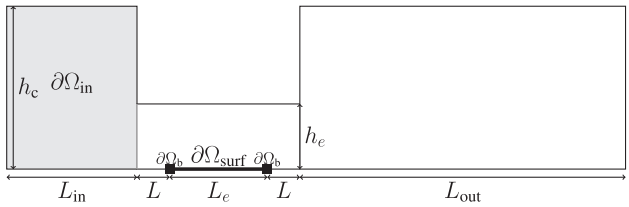

Fig. 4. PFMP and a schematic of the computational domain for the generalized reaction-diffusion continuum model. The parameters are defined in Table II. $\partial\Omega_b$ is the boundary of the tethered membrane illustrated by the black boxes, and $\partial\Omega_{in}$ is the analyte input flow-chamber indicted in gray.

1) Reaction Mechanism of PGLa: The chemical reactions leading to pore formation occur at the surface of the tethered membrane, denoted by $\partial\Omega_{\text{surf}}$. The conductance of the membrane $G_m(t)$ is dependent on the concentration of conducting pores in the membrane. To compute the concentration of conducting pores we consider the following reaction mechanism:

$$a \underset{k_d}{\overset{\mathbf{k_a^1}}{\rightleftharpoons}} m_1 \xrightarrow{k_p} p_1 \qquad np_1 \xrightarrow{k_1} p_n \qquad mp_n \xrightarrow{k_c} c, \quad (4)$$

where m_1 is the membrane-bound monomer, p_1 is the protomer, p_n is the conducting pore containing n protomers, and c is a closed pore. Note that after the peptide binds to the surface, it may undergo conformational and/or orientational changes prior to forming the pore. Once these changes have completed the monomer is denoted as a protomer. In (4) k_d is the dissociation constant, k_p is the rate of protomer formation, $\mathbf{k_a^1}$ the association rate constant, k_1 rate of protomer binding which includes the translocation of the peptide from the surface to the transmembrane orientation, and k_c the rate of pore closing with n and m denoting stoichiometric numbers. We define the association rate constant $\mathbf{k_a^1}$ as decreasing as the number of membrane-bound peptides increases. If we denote $m_{\max}$ as the maximum number of bound peptides, then the association constant is defined as $\mathbf{k_a^1} = k_a(m_{\max} - m_1 - p_1 - np_n - nmc)$. Note that if a was constant, then the surface binding mechanism in (4) resembles the "Langmuir-Hinshelwood" equation that is classically used to describe the dynamics of adsorption processes at surfaces.

Remark: The process of PGLa binding to the membrane surface (i.e. lipids) is a non-covalent molecular binding event. Such a bonding process can be modeled using coarse-grained molecular dynamics as no chemical bonds are formed between the PGLa and the lipids, however there is an attraction between the PGLa and the lipids such that the PGLa and lipids remain in close proximity to each other. This results as PGLa has an amphiphilic α-helical structure (e.g. the 4 positively charged

lysine residues on one side are hydrophilic and prefer to be adjacent to water, the residues on the other side are hydrophobic and are lipophilic which prefer to be adjacent to the lipid membrane). Given that PGLa has a charge of +4, the specific membrane binding mechanism is a combination of "non-specific hydrophobic association" and "peptide-lipid electrostatic interactions" for negatively charged membranes. The reaction mechanism (4) is a Hill-type approximation [21] of the aggregation and binding processes of the reaction mechanisms presented in [22] for α-Hemolysin pores, and in [23] for Cytolysin A pores. We do not consider the sequential binding (e.g. $2p_1 \rightarrow p_2$; $p_1 + p_2 \rightarrow p_3$;...; $p_1 + p_{n-1} \rightarrow p_n$) as a result of model identifiability–that is, if (4) is in agreement with the experimentally measured results, then a sequential binding process is guaranteed to fit the data with a series of slow binding steps followed by a fast binding step.

2) Electrolyte and Surface Diffusion of PGLa: The membrane conductance is dependent on the the chemical reactions and diffusion dynamics of PGLa. To model the diffusion dynamics of PGLa in solution we utilize a generalized version of Fick's law given by:

$$\frac{\partial a}{\partial t} = \nabla \cdot \left(D_a \nabla a + D_a a \nabla \ln \left(1 - N_{\mathrm{A}} r_a^3 a \right) \right), \qquad (5)$$

where a is the concentration of PGLa in solution, D_a is the diffusion coefficient of PGLa, N_{A} is the Avogadro's constant, and r_a is the effective radius of PGLa in solution. The maximum concentration of analyte possible is given by $a_{max} = 1/N_A r_a^3$ which assumes a cubic packing structure. Note that for (5) to be a suitable model, electrodiffusive effects must be negligible in the electrolyte. This assumptions holds for $F q_a u_a a \nabla \phi \ll 1$, where F is Faraday's constant, q_a is the charge of PGLa, and u_a is the ionic mobility PGLa. The generalized version of Fick's law includes a "Langmuir" type activity coefficient to account for the steric effects of PGLa–that is, the steric effects are accounted for by modifying the associated concentration. As seen, if $r_a = 0$ then we obtain the standard Fick's law of diffusion from (5).

In the membrane there exists surface bound PGLa with concentration m, protomer monomers, protomer dimers, higher order protomer complexes, and conducting pores, with concentrations given by: $a, m, p_1, p_2, \ldots, p_n$. The dynamics of the PGLa peptide complexes in the membrane are governed by the following surface reaction-diffusion partial differential equations:

$$\begin{aligned}
\frac{\partial m}{\partial t} &= \nabla_s \cdot J_m + R_m, \\
J_m &= \left(D_m \nabla_s m + D_m m \nabla \ln \left(1 - N_{\mathrm{A}} (r_m^2 m + \sum r_i^2 p_i) \right) \right), \\
\frac{\partial p_i}{\partial t} &= \nabla_s \cdot J_i + R_i, \\
J_i &= \left(D_i \nabla_s p_i + D_i p_i \nabla \ln \left(1 - N_{\mathrm{A}} (r_m^2 m + \sum r_i^2 p_i) \right) \right), \\
&\text{for } i \in \{1, 2, \ldots, n\}. \qquad (6)
\end{aligned}$$

In (6) ∇_s is the surface gradient, D is the surface diffusion coefficient of the respective species, r is the effective radius of each species, and R_m denotes the change in concentration as a result of PGLa binding to the membrane surface, and R_i the subsequent chemical reactions leading to pore formation. The boundary conditions of (5) and (6) are given by:

$$\begin{aligned}
&n \cdot D_a \nabla a = R_a \text{ in } \partial\Omega_{\mathrm{surf}}, \qquad n \cdot D_a \nabla a = 0 \text{ otherwise}, \\
&n \cdot D_m \nabla_s m = 0 \text{ in } \partial\Omega_{\mathrm{b}}, \qquad n \cdot D_i \nabla_s p_i = 0 \text{ in } \partial\Omega_{\mathrm{b}}. \qquad (7)
\end{aligned}$$

with $\partial\Omega_{\mathrm{surf}}$ the membrane surface, and $\partial\Omega_{\mathrm{b}}$ the boundary of the membrane surface, and n the unit normal vector. In (7), R_a denotes the binding process of the PGLa peptide in solution to the membrane-bound state m. The chemical reaction rates R_a, R_m, and R_i can be computed from reaction mechanism (4). Initially the solution of PGLa with concentration a_o is inserted into a flow-cell chamber defined by $\partial\Omega_{\mathrm{in}}$. The initial conditions of (5) and (6) are given by:

$$\begin{aligned}
&a|_{t=0} = a_o \text{ in } \partial\Omega_{\mathrm{in}}, \qquad a|_{t=0} = 0 \text{ otherwise}, \\
&m|_{t=0} = 0 \text{ in } \partial\Omega_{\mathrm{surf}}, \qquad p_i|_{t=0} = 0 \text{ in } \partial\Omega_{\mathrm{surf}}. \qquad (8)
\end{aligned}$$

The conductance of the membrane is dependent on the concentration of conducting PGLa pores and the equilibrium number of aqueous pores in the membrane resulting from random thermal fluctuations. Denoting G_o as the conductance of the aqueous pores, then the total conductance of the membrane is given by:

$$\hat{G}_m(t) = G_o + \kappa_p \int_{\partial\Omega_{\mathrm{surf}}} p_n(t, x) dS. \qquad (9)$$

In (9), κ_p is a proportionality constant relating the mean conductance of the pores to the molar concentration of pores p_n. The mean conductance of each PGLa pore G_p (Fig. 1) is equal to $\kappa_p / N_{\mathrm{A}}$ where N_{A} is Avagadro's constant. From experimental measurements and theory G_p is expected to be in the range of pS-nS [24], [25].

Given the initial concentration a_o, the diffusion coefficients D from coarse-grained molecular dynamics, the governing equations (5) and (6) with the boundary conditions (7) and initial conditions (8), the conductance of the membrane can be estimated using (9). Given measurements, the experimental membrane conductance denoted $G_m(t)$, can be evaluated as the solution of the fractional order macroscopic model. Then least squares estimates of the reaction rate constants $R_a(t)$, $R_m(t)$, $R_i(t)$ that describe the pore formation reaction mechanism can be obtained by minimizing $(G_m(t) - \hat{G}_m(t))^2$ at each time t.

C. Coarse-Grained Molecular Dynamics

The CGMD model is used to gain insight into the reaction mechanism and dynamics leading to PGLa pore formation, and the diffusion coefficients D in (6). For studying the dynamics of PGLa binding, insertion, and oligomerization requires a simulation size of tens of nanometers with a simulation time horizon of several microseconds [26]. All-atom molecular dynamics is practically limited for this system size and simulation time, however using CGMD allows a 2-3 orders of magnitude increase in both system size and simulation time compared to all-atom molecular dynamics simulations [27]. Therefore, we

employ the non-polarizable MARTINI force-field [26], [28] to perform all CGMD simulations in [13]–[15], [29]–[33]. Note that the CGMD model is validated in Sec.III using results from the all-atom molecular dynamics simulation in [13]–[15], [29]–[33]. Note that the CGMD model is not utilized to study the formation process of aqueous pores (i.e. water filled pores formed by ionic gradients), for details on the formation process of aqueous pores the reader is referred to [34], [35].

The antimicrobial peptide PGLa contains 21-residues with amino-acid sequence (GMASKAGAIAGKIAKVALKAL -NH_2). As a result of recent advances in ^{2}H-NMR, ^{15}N-NMR, and ^{19}F-NMR spectroscopy [36]–[42] it is known the PGLa peptide has a α-helical configuration when membrane-bound. The transmembrane state of PGLa (i.e. the long axis of the peptide is parallel to the membrane normal) has not been observed at physiological temperatures with NMR as the lifetime of conducting pores is too short for NMR measurement [42]–[44]. However from recent NMR measurements [42] when a 1:1 mixture of PGLa and Maginin 2 is used, the PGLa has been observed in the transmembrane state and retains the α-helical structure. Though the transmembrane configuration of PGLa, with no additional peptide present, has not been observed experimentally, it is suggested that for high peptide to lipid ratios the configuration of the transmembrane PGLa monomer retains the α-helical structure [44], a common trait of similar α-helical peptides including Alamethicin [45], Maginin 2 [46], and Melittin [47]. Additionally it is known that amine-terminus and carboxyl-terminus of antimicrobial peptides are thermodynamically stable (i.e. local energy minimum) when in contact with the surface of the membrane [48]. Therefore, for all CGMD simulations the secondary structure of the PGLa is constrained to have a α-helical structure.

The all-atom PGLa is constructed using the software Molefacture contained in VMD [49]. The secondary-structure of the membrane-bound PGLa is defined by a α-helix with $\phi = -57°$ and $\psi = -47°$. The all-atom PGLa is coarse-grained for use with the MARTINI force field using the protocol described in [27] with each CGMD bead representing approximately four heavy atoms. A schematic of the all atom structure of PGLa and coarse-grained PGLa structure are provided in Fig. 5. The membrane is modeled using 512 DphPC CGMD molecules. The parameters of the CGMD model and setup for the surface binding, translocation of surface bound to transmembrane bound, and oligomerization are provided in Appendix C.

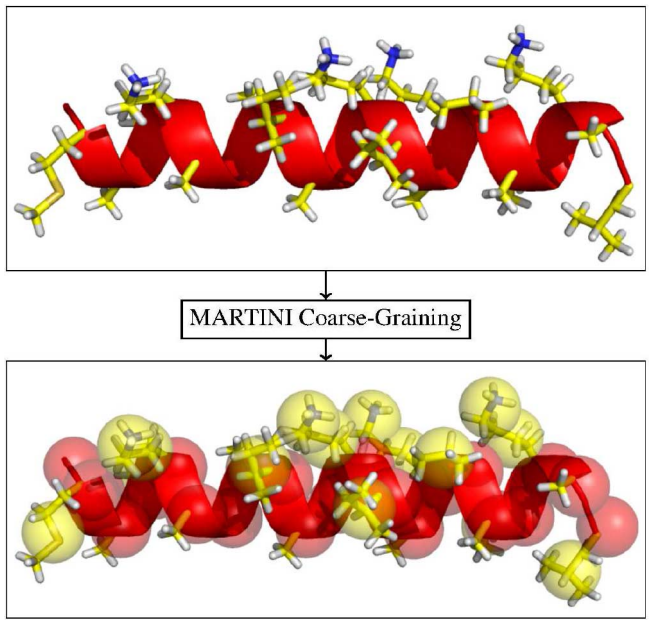

Fig. 5. Schematic of the all-atom structure of PGLa (GMASKAGAIAGKIAKVALKAL-NH_2) and the corresponding MARTINI coarse-grained structure constructed using the protocol in [27]. The PGLa backbone beads are displayed in red, and side chain beads in yellow.

III. Numerically Predicted Dynamics of PGLa

In this section we estimate the chemical kinetics of PGLa pore formation using the PFMP and mesoscopic-to-observable model constructed in Sec.II. The CGMD model parameters and setup are provided in Appendix C.

A. Diffusion of PGLa and Membrane Properties from Coarse-Grained Molecular Dynamics

The surface bound and transmembrane diffusion coefficients of PGLa play a central role in the dynamics of PGLa pore formation in biological membranes (refer to (5) and (6)). To estimate these important parameters we use the CGMD model of PGLa. The diffusion coefficients for surface bound and transmembrane bound monomers, dimers, and trimers is provided in Table I. As expected the diffusion coefficient of the PGLa protomers decrease as the number of monomers in each protomer increases. Interestingly the diffusion coefficients for the transmembrane protomers satisfy the "free-drain limit" [50] in which the diffusion coefficient satisfies $D_n = D_i/n$ within the error bounds. This effect has been observed for membrane-bound proteins using single-molecule fluorescence spectroscopy techniques [51]. We do not consider the diffusion of higher order protomers as the CGMD model results are in agreement with the experimentally measured results for PGLa protomers containing up to three monomers.

TABLE I
Diffusion Coefficients of PGLa Protomers (μm^2/s)

	Monomer	Dimer	Trimer
Transmembrane	91.2 ± 19.5	41.8 ± 16.0	26.25 ± 9.0
Surface Bound	127.5 ± 12.4	50.7 ± 14.4	21.0 ± 8.0

The diffusion of PGLa (Table I) is dependent on the accuracy of the CGMD model of the DphPC lipid bilayer. To validate the DphPC model we compare the lipid and water diffusion coefficients, membrane thickness, area per lipid, and the aliphatic chain deuterium order parameter [29]–[31] of the lipids. The diffusion coefficient of the DphPC lipids is 84.9 ± 0.2 μm^2/s, in excellent agreement with the expected range of 10-100 μm^2/s [33]. The estimated diffusion of water is 2.00 ± 0.02 nm^2/ns, in agreement with the experimentally measured diffusion coefficient of water 2.30 nm^2/ns [52]. The computed thickness of the membrane is 4.0 ± 0.1 nm, which is in agreement with the molecular dynamics results in [13]–[15], [29]–[32] which are in the range of 3.6 to 4.0 nm. The estimated area per DphPC lipid is 62.3 ± 0.3 Å^2, in agreement with

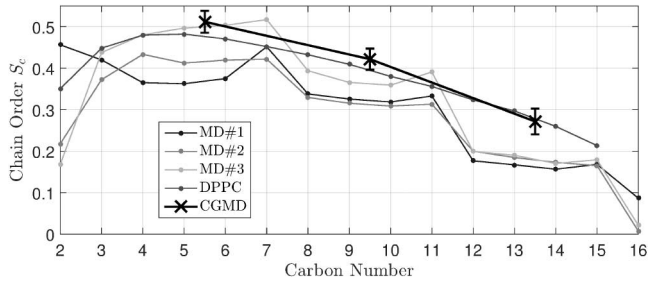

Fig. 6. Computed chain order S_c (Appendix C) from the CGMD model, and the aliphatic chain deuterium order parameter from the molecular dynamics simulations of ester-DphPC, ether-DphPC, and DPPC [29]–[31] scaled by a factor of -2. The error bars on the CGMD markers indicate the associated error for each data point. For the ester-DphPC molecules (MD#1,MD#2) and ether-DphPC molecules (MD#3), the carbon numbers (3, 7, 11, 15) are attached to the methyl groups with 16 denoting the terminal methyl, and for DPPC carbon 15 represents the terminal carbon of the aliphatic chain.

the molecular dynamics results reported in [13]–[15], [29]–[32] which range from 62 to 80 Å^2. How does the deuterium order parameters S_{CD} [29]–[31] from molecular dynamics compare with the lipid order in the CGMD model S_c (refer to Appendix C for definition of S_{CD} and S_c)? From Fig. 6 we see that results from the CGMD model are in reasonable agreement with the deuterium order parameters from molecular dynamics for ester-DphPC and DPPC membranes. Note that results from molecular dynamics have illustrated that the order parameters for ether-DphPC lipids have a higher order parameter then the ester-DphPC [32]. Therefore, given that the CGMD model is constructed using ether-DphPC, it is expected that the CGMD model would have higher order parameters compared with the ester-DphPC lipids. The results in Fig. 6 also suggest that ether-DphPC lipids have a higher order parameter then the DPPC lipids. This results as the aliphatic chains in ether-DphPC form a tightly packed network with neighbouring hydrocarbon chains being interdigitated which results in an increase in their order parameter compared to that of DPPC [32].

B. Surface Binding and Oligomerization of PGLa From Molecular Dynamics

In this section the CGMD model of PGLa is used to gain insight into the mechanism of surface binding, translocation of surface bound peptides to the transmembrane state, and oligomerization. Surface binding and entry into the transmembrane state are key steps in the pore formation reaction mechanism presented in Sec.II-B.

Fig. 7 presents the surface binding, translocation, and oligomerization processes of PGLa in a DphPC membrane. An explanation of each reaction mechanism is provided below.

1) Surface Binding of PGLa: Following the method presented in [36] for monomer insertion, the PGLa monomer is initially placed above the DphPC membrane with an α-helix configuration. Recall from Sec.II-C that the membrane-bound secondary-structure of PGLa is α-helical as measured experimentally from NMR spectroscopy [43], [44], [53]–[55]. The peptide to lipid ratio of the monomer binding is 1:512. As seen in Fig. 7 the amine-terminus of the PGLa monomer first

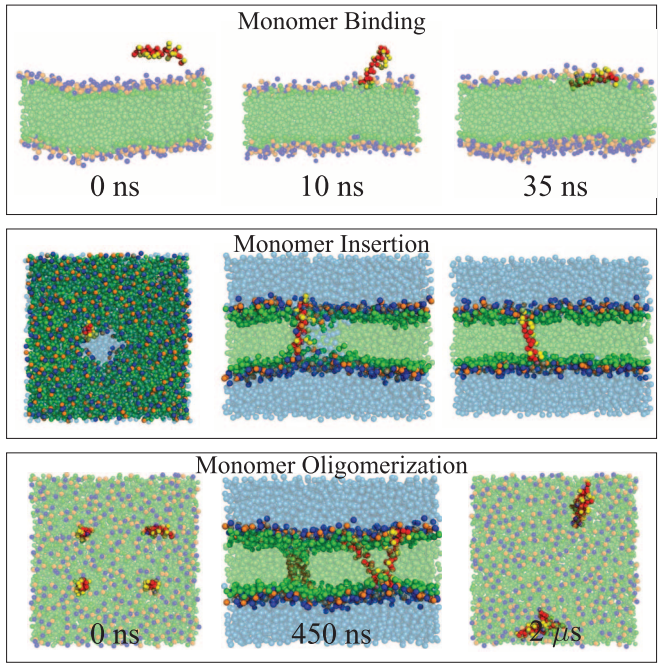

Fig. 7. Snapshots of CGMD bead positions for the surface binding, translocation, and oligomerization of PGLa in a DphPC membrane. The NC_3 bead is displayed in blue, the PO_4 bead in orange, the lipid tail carbons in green beads, the PGLa backbone beads in red, PGLa side chains using yellow beads, and water using light blue beads. The CGMD setup and parameters are defined in Appendix C.

binds to the surface of the DphPC membrane. At 20 ns the PGLa monomer pivots on the amine-terminus and begins to embed itself into the membrane surface. The final surface bound structure of the PGLa monomer is reached at 35 ns with the charged lysine residues pointing into the bulk electrolyte and the hydrophobic region in contact with the hydrophobic phytanyl tails of the DphPC membrane. The monomer remains in the membrane until the simulation horizon is reached at 1 μs. The computed tilt angle, defined as the angle between the helix long-axis vector and the membrane normal, of the PGLa monomer is $90 \pm 5°$ which is in excellent agreement with the ^{2}H-NMR results of approximately 95° [42] and the results from molecular dynamics [36].

2) PGLa Translocation to Transmembrane State: How do the peptides transition from the surface bound state to the transmembrane state? For a 1 μs CGMD simulation we did not observe the surface bound monomer (Fig. 7) transition to the transmembrane state. The reason this occurs is that in molecular dynamics models [36], the surface bound peptide orientation is persistent. As shown in [48] using potential of mean force computations for similar length (19 residue) α-helical peptides, the transition from the surface bound state to the transmembrane state is not energetically favored. If however, a transient aqueous pore exists in the membrane, then the PGLa can diffuse into the transient pore. A population of transient aqueous pores exist in all membranes as a result of random thermal fluctuations [18]. From Fig. 7, once a transient aqueous pore has formed, the PGLa monomer diffuses into the walls of the aqueous pore. As the transient pore closes the PGLa monomer enters the transmembrane state. The

monomer remains in the transmembrane state for the remainder of the simulation. As expected from the results in [48], the PGLa is in a thermodynamically stable conformation when transmembrane bound. The transmembrane structure of PGLa has not been observed by NMR spectroscopic at physiological temperatures possibly as a result of the PGLa pores being transient [42]. In a gel-phase DMPC/DMPG bilayer at temperatures below 15 °C, NMR measurements show that PGLa is in a transmembrane state with a tilt angle of approximately 180° [43]. This is in agreement with the tilt angle of the transmembrane PGLa monomer which has a tilt angle of $168 \pm 5°$–the difference in angle is a result of the gel-phase DMPC/DMPG bilayer having a larger membrane thickness then the DphPC membrane which is in the liquid phase.

3) Oligomerization of PGLa: From the reaction mechanism (4), a necessary step for PGLa pore formation is an oligomerization process. Is it possible for PGLa peptides in the transmembrane state to oligomerize in the DphPC membrane? To study if the transmembrane PGLa oligomerize we initially setup a DphPC membrane with four embedded PGLa peptides as illustrated in Fig. 7. Initially the monomers diffuse in the membrane. As time progresses the monomers form transmembrane dimers. The formation of the transmembrane dimers from the monomers are dependent on the orientation and diffusion dynamics of the peptides, as such the first dimer is formed at 150 ns, and the second at 450 ns. The formation of the two dimers occur as a result of the amine-terminus or carboxyl-terminus interacting when two peptide come into close contact. The four PGLa monomers have formed two transmembrane dimers remain stable for the duration of the simulation. Can these two dimers bind to form a quadramer complex? Over a 4 μs simulation the two dimers where not observed to form a quadramer complex. A possible explanation is the arrangement of the +4 charged lysine residues on the PGLa. In the PGLa dimer, the hydrophilic face of each PGLa monomer prefers to face the hydrocarbon interior of the membrane. If we consider the energy required to bring the +4 charged lysine residues in close proximity, it is not surprising that this conformation is preferred for the dimer structure. Given that the two dimers contain +4 charged lysine residues facing outwards, and that the dimers prefer to have the lysine residues oriented towards the hydrocarbon interior, the possibility of a quadromer forming from two dimers is unlikely.

What are the possible oligomerization steps necessary to form a transmembrane PGLa trimer? Once a PGLa dimer has formed (Fig. 7), then it is possible for a transmembrane bound PGLa monomer to bind with the dimer to form a transmembrane PGLa trimer. The formed trimer is illustrated in Fig. 8. The results in Fig. 8 suggest that the amine-terminus of the PGLa monomer stabilizes the trimer while the carboxyl-terminus contributes negligibly to the binding of the three PGLa monomers. However the carboxyl-terminus may promote the passage of ions through the membrane by causing local membrane instabilities increasing the conductance of the membrane. The formed PGLa trimer remains stable for the duration of the simulation.

The results in Fig. 7 and Fig. 8 provide snapshots of a possible reaction mechanism (4) for PGLa. To estimate the associated rate constants in (4) requires experimental measurements from the PFMP and the dynamic model presented in Sec. II.

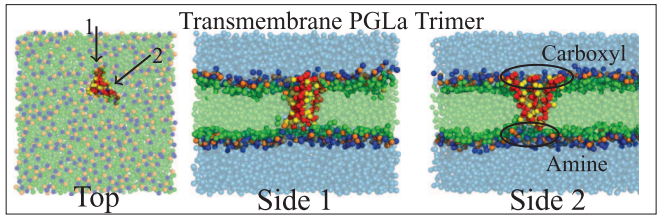

Fig. 8. Snapshots of CGMD bead positions for the transmembrane PGLa trimer. To illustrate the PGLa trimer structure two side views are displayed, each denoted by 1 and 2. The CGMD setup and parameters are defined in Appendix C.

IV. Experimentally Measured Dynamics of PGLa in Engineered Tethered Membrane

In this section insight into the reaction mechanism of PGLa is provided using experimental measurements from the PFMP and dynamic model presented in Sec. II. Prior to all experimental measurements the quality of the PFMP is verified using impedance measurements. We study the PGLa pore formation dynamics for varying concentrations of PGLa and with membranes containing different charges–this mimics the physiological response of PGLa to negatively charged membrane surfaces. Details on the experimental measurements and numerical methods are provided in Appendix A and B.

A. Quality of Tethered Membrane

Prior to all experimental measurements the impedance of the tethered membrane is measured. This allows us to detect if the membrane contains significant defects. Possible membrane defects include patches with the gold electrode directly exposed to the bulk electrolyte, or with portions of bilayer sandwiched together. The defect density in the membrane can be estimated from the impedance measurements using the protocol presented in [56]. If the estimated capacitance of the membrane significantly increases this indicates that either electrodesorption of the tethers and spacers has occurred, or portions of the tethered membrane have been released into the electrolyte. If the estimated equilibrium aqueous pore conductance significantly increases then catastrophic voltage breakdown of the membrane has occurred causing separated areas of the membrane to degrade. Typical values for membrane capacitance and conductance are $0.5 - 1.3$ μF/cm^2 and $0.5 - 2.0$ μS for an intact 10% tethered membrane with surface area 2.1mm^2. The estimated fractional order parameter lies in the range between 0.8 and 0.9; therefore, a diffusion-limited process is present at the surface. This is likely caused by a combination of diffusion-limited charge transfer, quasireversible charge transfer, and ionic adsorption is present at the surface of the gold electrodes. These double-layer charging effects can be modeled using fractional order operators [16]. For all experimental measurements, the membrane contained negligible defects. Fig. 9 presents an example of the experimentally measured and numerically

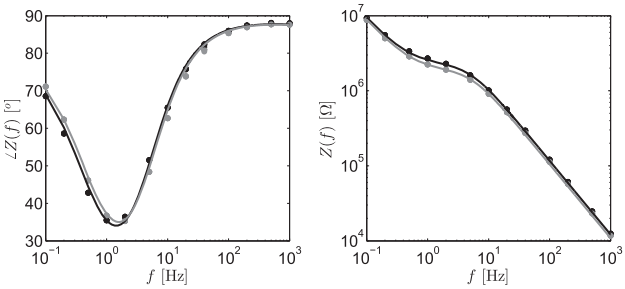

Fig. 9. The measured and predicted impedance (phase is represented by $\angle Z(f)$ in degrees and magnitude by $Z(f)$) of the 10% tether density DphPC bilayer membrane. The solid line is the predicted and the dotted the experimentally measured. The grey and black colours indicate the impedance for two identically constructed membranes. All predictions are computed using (3). The experimental results are extracted from [18].

predicted impedance for the tethered membrane. As seen, the predicted impedance is in excellent agreement with the experimentally measured impedance and is consistent with a membrane containing negligible defects.

B. Reaction Dynamics of PGLa

In Fig. 10 the experimentally measured and numerically predicted conductance for varying concentrations of PGLa are presented. The mean-absolute percentage error for the experimentally measured and numerically predicted conductance in Fig. 10 is 3.7%–that is, the predicted and measured conductance are in excellent agreement. Initially the conductance increases as a result of PGLa peptides diffusing to the membrane surface, binding, translocation to the transmembrane configuration as illustrated in Fig. 7. As shown in Fig. 10, at about 500 s the conductance of the membrane begins to decrease. This suggests that PGLa pores begin to close and prevent the formation of new PGLa pores. Given PGLa has a positive charge of +4 as a result of the lysine residues, as the membrane becomes saturated with PGLa this causes the overall charge of the membrane to decrease inhibiting the insertion of PGLa into the membrane. The estimated PGLa pore conductance G_p is in the range of 0.6 to 3.5 pS, in agreement with the expected pore conductance from [24], [25]. As expected the association coefficient k_a (4) is four orders of magnitude larger then the protomer formation rate constant k_p. This is expected as the binding of the PGLa to the surface (Fig. 7) does not require the translocation of the peptide to the transmembrane state. As suggested from the results in Fig. 7, the translocation likely involves the peptide diffusing into a transient aqueous pore which is a slower process then the peptide directly binding to the surface. The rate of closing k_c (4) is large suggesting that PGLa pores only form transiently in the uncharged membrane. This provides an explanation for why the transmembrane state of the PGLa has not been observed at physiological temperatures using NMR techniques [43]. The estimated solution diffusion coefficient of PGLa (D_a in (5)) is in the range of 2 nm^2/ns to 5 nm^2/ns. As expected, the analyte diffusion coefficient D_a is a factor of 10-100 larger then the surface bound and transmembrane bound PGLa monomers, dimers, and trimers in Table I.

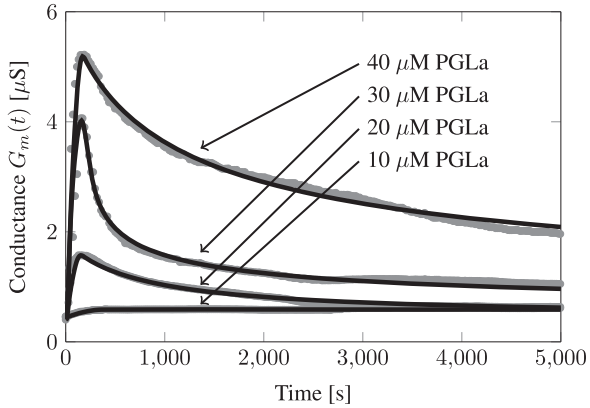

Fig. 10. Experimentally measured and numerically predicted conductance for DphPC tethered membrane with 10, 20, 30, and 40 μm of PGLa. The predictions are made using (5), (6) with the reaction mechanism given by (4) and simulation parameters provided in Table III. The experimental results are extracted from [57].

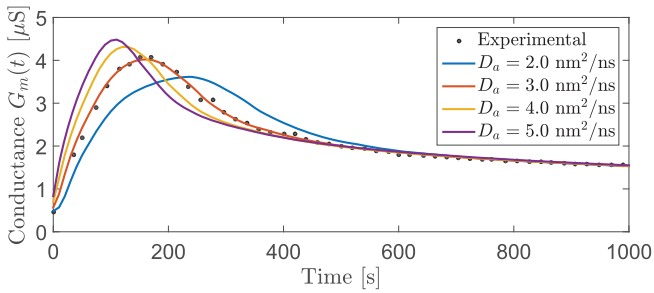

Fig. 11. Experimentally measured conductance for DphPC tethered membrane with 30 μM of PGLa, and numerically predicted conductance with varying D_a values. The predictions are made using (5), (6) with the reaction mechanism given by (4) and simulation parameters provided in Table III. The experimental results are extracted from [57].

How sensitive is the membrane conductance $G_m(t)$ to variations in the analyte diffusion coefficient D_a? To gain insight into how D_a impacts $G_m(t)$, Fig. 11 provides $G_m(t)$ for D_a in the range of 2 nm^2/ns to 5 nm^2/ns. From Fig. 11 it is clear that $D_a = 3$ nm^2/ns provides a resulting $G_m(t)$ which that is in agreement with the experimental measurements for the 30 μM PGLa interaction with the DphPC membrane. For large D_a the conductance increases faster, however the formed PGLa pores also close faster then compared to the $D_a = 3\,\text{nm}^2/\text{ns}$ case. The reverse effect is observed for $D_a < 3\,\text{nm}^2/\text{ns}$ as seen in Fig. 11. Note that although the membrane conductance is strongly dependent on D_a, $G_m(t)$ is negligibly dependent on the surface and transmembrane bound diffusion coefficients (D_i in (6)) of PGLa. This results because $D_i \ll D_a$ such that the reaction-diffusion equation in (6) can be approximated by a set of distributed non-linear ordinary differential equations.

To gain insight into the effect the membrane charge has on the dynamics of PGLa pore formation, a membranes with varying concentration of charged POPG lipids are constructed. Fig. 12 presents the response of the 10% tethered membrane with charged (POPG lipids) and uncharged (DphPC) lipids resulting from the addition of 30 μM PGLa. As seen the numerically estimated results are in excellent agreement with the

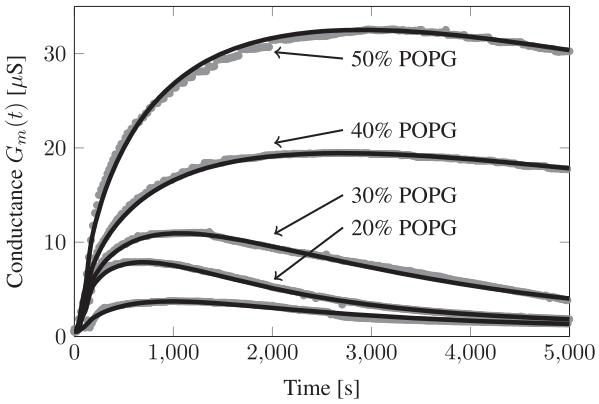

Fig. 12. Experimentally measured (dotted) and numerically predicted (solid line) membrane conductance for tethered membranes composed of 10%, 20%, 30%, 40%, and 50% POPG with a PGLa concentration of 30 μM. The predictions are made using (5), (6) with the reaction mechanism given by (4) and simulation parameters provided in Tables I–III. The experimental results are extracted from [57].

experimentally measured conductance. As expected, the negatively charged POPG lipids promote the binding of positively charged PGLa peptides–as % of POPG lipids increase the membrane conductance increases. In comparing Fig. 10 with Fig. 12, it is clear that PGLa has an affinity for forming pores in biological membranes containing negatively charged lipids typically found in prokaryotic cells. Using the reaction rate model we find that the rate of protomer formation k_c in (4) increases as the negative charge of the membrane increases. However, the rate of pore closure (k_c in (4)) decreases as the negative charge of the membrane increases. This suggests that as the negative charge of the membrane increases there is an increase in the number of PGLa pores and pore lifetime. This makes PGLa especially effective for disrupting and perforating biological membranes containing a net negative charge.

V. Conclusion

This paper has presented a mesoscopic-to-observable model of the PFMP for the study of the pore formation dynamics of antimicrobial peptides. The model is composed of three levels of abstraction: a fractional order macroscopic model which accounts for diffusion limited processes at the bioelectronic interface of the PFMP, a generalized reaction-diffusion continuum model which models the pore formation dynamics of peptides, and a coarse-grained molecular dynamics model which is used to compute continuum parameters and estimate the pore formation reaction pathway. The computed results from the mesoscopic-to-observable model are in agreement with the experimentally measured results from the PFMP for PGLa interacting with an uncharged DphPC membrane, and a charged POPG membrane. The results from the coarse-grained molecular dynamics model suggest that PGLa can bind to the membrane surface, transition to the transmembrane conformation via transient aqueous pores, and oligomerize once in the transmembrane conformation. Using the mesoscopic-to-observable model and experimental measurements suggests that PGLa preferentially targets and increases the permeability of biological membranes containing a net negative charge–that is, PGLa not only increases the number of pores in negatively charged membranes, but the lifetime of conducting pores also increases compared to the lifetime of PGLa pores in uncharged membranes. Though we apply the PFMP and mesoscopic-to-observable model to the study of pore formation dynamics of PGLa, the platform and modeling methodology are general and can be used for other pore forming peptides and proteins of interest.

Appendix A
Experimental Parameters

All experimental measurements were performed at a temperature of 20° C in a phosphate buffered solution with a pH of 7.2 and a saline solution of 0.15 M composed of Na^+, K^+, and Cl^-. A pH of 7.2 was selected to match that typically found in the cytosol of biological cells. The formation of the tethered bilayer lipid membrane can be found in [11], [18]. The negatively charged palmitoyl-oleoyl-phosphatidylglycerol (POPG) lipid membrane was constructed using an ethanolic solution containing archaebacterial lipids (70% zwitterionic C20 diphytanyl-ether-glycero-phosphatidylcholine lipid and 30% C20 diphytanyl-diglyceride ether) mixed with 0-50% POPG lipids. The impedance of the PFMP is recorded using a tethaPod (SDx Tethered Membranes) which measures the impedance using a 20 mV excitation at frequencies of [1000, 500, 200, 100, 40, 20, 10, 5, 2, 1, 0.5, 0.2, 0.1] Hz. The antimicrobial peptide PGLa was synthesized using solid-phase Fmoc protocols [58], [59] on an Applied Biosystems (Carlsbard, CA) 433A instrument using a reverse-phase HPLC [60].

Appendix B
Continuum Model: Numerical Method and Parameters

The governing equations (5) and (6) with boundary conditions (7) and initial conditions (8), are solved numerically with the commercially available finite element solver COMSOL 5.0 (Comsol Multiphysics, Burlington, MA). The simulation domain is meshed with approximately 28,199 triangular elements constructed using an advancing front meshing algorithm. Eq. (5) and (6) are numerically solved using the *multifrontal massively parallel sparse direct solver* [61] with a variable-order variable-step-size backward differential formula [62]. Eq. (9) is used to compute the pore conductance with the integration performed on $\partial\Omega_{\text{surf}}$. The computational domain of the continuum model is provided in Fig. 4 with the parameters defined in Table II.

The maximum concentration of PGLa in solution is computed by multiplying the molecular weight of PGLa (1970 g/mol) by the average protein specific volume of $0.73\,\text{cm}^3/\text{g}$ [63]. The maximum concentration of PGLa in solution is 695 mM–this corresponds to $r_a = 1.33$ nm in (5). The maximum surface concentration of membrane-bound PGLa and protomers is taken as corresponding to 1% of the total molar concentration of the tethered membrane lipids. Each lipid in the tethered membrane has a surface area of $0.62\,\text{nm}^2$, therefore

TABLE II
GEOMETRIC PARAMETERS OF PFMP (FIG.4)

Symbol	Definition	Value
h_c	Inlet chamber height	4 mm
L_{in}	Inlet chamber length	2 mm
L	Channel buffer length	1 mm
h_{e}	Channel height	0.1 mm
L_e	Electrode length	0.7 mm
L_{out}	Outlet chamber length	20 mm
h_{out}	Outlet chamber height	4 mm

TABLE III
PARAMETER VALUES FOR VARYING PGLA (FIG. 10)

Symbol	Definition	Value
r_a	Effective radius of PGLa	1.33 nm
m_{max}	Saturated surface concentration	5×10^{-10}
k_a	Adsorption rate constant	5000 m^2/smol
k_d	Desorption rate constant	0 1/s
k_d	Desorption rate constant	0 1/s
k_p	Rate of protomer formation	0.5 1/s
k_1	Rate of protomer binding	0.5 1/s
n	n in (4)	1
D_a	Analyte diffusion coefficient	2-5 nm^2/ns
PGLa concentration a_o	m in (4)	k_c in (4)
10 μM	2	1×10^2 m^2/smol
20 μM	2	1.2×10^6 m^2/smol
30 μM	3	26×10^{15} m^4/smol^2
40 μM	3	1.1×10^{15} m^4/smol^2

for a $2.1\,\text{mm}^2$ membrane there are approximately 3×10^{12} lipids in the surface layer. Therefore the maximum surface concentration of membrane-bound PGLa and protomers is 2.5×10^{-8} mol/m^2. This corresponds to an effective surface radius for each membrane-bound PGLa and protomer (i.e. r_m and r_i in (6)) to be 8 nm. The maximum surface concentration for PGLa m_{max}, defined below (1), was selected to match that of the maximum surface concentration of Cytolysin A [23]. The reaction-diffusion parameters for numerical results presented in Fig. 10 and Fig. 12 are provided in Tables I–III respectively.

APPENDIX C
COARSE-GRAINED MOLECULAR DYNAMICS: METHOD AND PARAMETERS

All CGMD simulations were implemented in GROMACS version 4.6.2 [64]–[66]. For all production runs the Berensden temperature coupling is used with a temperature of 323 K, and a time constant of 0.3 ps. A temperature of 323 K was selected to ensure that the CGMD water does not freeze [26], [28]. The Berendsen semi-isotropic pressure coupling is used with a time constant of 3.0 ps, compressibility of 3×10^{-5} 1/bar, and a reference pressure of 1.0 bar [67]. The timestep of the simulation is 20 fs with the electrostatic interactions smoothly shifted from zero at 12Å and Lennard-Jones interaction from 9−12Å. The membrane is modelled using 512 dipalmitoylphosphatidylcholine (DPPC) molecules. Note that DPPC has an identical structure to DphPC, and a similar structure to GDPE when using the CGMD representation as mesoscopic details such as the phytanyl tails in the DphPC and GDPE are equivalent to the palmitoyl tails in DPPC. The 512 lipid CGMD DphPC membrane is constructed by replicating the equilibrated 128 DPPC bilayer, from the MARTINI website[1], twice in the X and Y directions. The 512 DphPC membrane is solvated using CGMD water beads and energy minimized followed by an equilibration in NPT for 200 ns to produce the equilibrated membrane structure. The dimensions of the simulation cell containing the membrane are 126Å × 129Å × 150Å corresponding to X × Y × Z coordinate axis. The solvent solution surrounding the peptide and membrane surface is composed of water molecules and Na^+ and Cl^- ions to make the solvent a 0.15 M NaCl solution and also to neutralize the charge on the peptides.

Surface Binding of PGLa: To study the monomer binding of PGLa to the membrane surface (Fig. 7), a single PGLa peptide is placed 17Å above the surface of the membrane. After energy minimization, the production run was carried out for a simulation time horizon of 1 μs.

Transmembrane Insertion of PGLa: To construct the transient aqueous pores in Fig. 7 which allow the PGLa to translocate from the membrane surface to the transmembrane state, we employ the method outlined in [68] to construct the aqueous pore. The Berendsen semi-isotropic pressure coupling is used with a time constant of 3.0 ps, compressibility of 3×10^{-5}1/bar, and a reference pressure of 1.0 bar in the direction normal to the membrane surface. The lateral pressure is held at −50 bar until a transient pore has formed. The negative pressure promotes the formation of transient aqueous pores in the membrane. After a transient pore has formed and the PGLa has diffused into the aquous pore, the lateral pressure is set to 1.0 bar allowing the aqueous pore to close. The production run for pore closure has a simulation time horizon of 500 ns.

Oligomerization of Transmembrane PGLa: To study the oligomerization process of PGLa we place four PGLa monomers in the transmembrane state, as illustrated in Fig. 7, using the method outlined in [45]. PyMOL (The PyMOL Molecular Graphics System, Version 1.3 Schrödinger, LLC) is used to place the peptides in the transmembrane state in the membrane. The system is equilibrated in the NPT ensemble for 20 ns. After energy minimization the production run is carried out for 4 μs.

Diffusion: To estimate the diffusion of water, lipids, and PGLa complexes we compute the ensemble-averaged time-dependent mean square displacement (MSD) $\langle (x - x_o)^2 \rangle$ with x_o denoting the initial position, x the position of the complex t later, and ensemble average taken over time. The MSD is computed with respect to the center-of-mass of the molecule. The MSD is related to the diffusion coefficient by $\langle (x - x_o)^2 \rangle = 4D(t - t_o)$. To reduce the noise of the estimated diffusion D, we average the MSD of sub-trajectories of t, as done in [69]. The setup for the surface bound and transmembrane bound dimer and trimers are provided below. To construct the surface bound PGLa dimer, two PGLa monomers are placed 17Å above the membrane surface separated by 22Å. A production run was carried out for sufficient time to allow the formation of the PGLa dimer. The surface bound trimer is constructed using an identical procedure with three PGLa monomers. To construct the PGLa trimer, three PGLa monomers are placed in the

[1] http://md.chem.rug.nl/cgmartini/index.php/downloads

transmembrane state, then after energy minimization allowed to oligomerize until the transmembrane trimer has formed. The diffusion coefficient are computed from production runs of 1 μs.

Order Parameter: Popular parameters for characterizing the order in lipid bilayers is the deuterium order parameters S_{CD} [29]–[31] for aliphatic chains and is given by $S_{\mathrm{CD}} = (3\langle\cos^2(\theta)\rangle - 1)/2$ where θ is the angle between the carbon to hydrogen vector and the membrane normal with $\langle\cdots\rangle$ denoting the time-average. The order parameter $S_{\mathrm{CD}} = 1$ when there is perfect alignment of the bond with the bilayer normal, and zero indicates the bond has a completely random orientation. For the CGMD model, to estimate the order of the lipid bilayer we compute the order of the chains $S_c = (3\langle\cos^2(\theta_c)\rangle - 1)/2$ where θ_c is the angle between the vector of the two nearest-neighbor beads, and the membrane normal. Note that S_{CD} and S_c are related by $S_c = -2S_{\mathrm{CD}}$ allowing us to compare the order parameter results from molecular dynamics and NMR to the results from the CGMD model [70].

REFERENCES

[1] M. Zasloff, "Magainins, a class of antimicrobial peptides from Xenopus skin: Isolation, characterization of two active forms, and partial cDNA sequence of a precursor," *Proc. Nat. Acad. Sci.*, vol. 84, no. 15, pp. 5449–5453, 1987.

[2] M. Baker, W. Maloy, M. Zasloff, and L. Jacob, "Anticancer efficacy of magainin2 and analogue peptides," *Cancer Res.*, vol. 53, no. 13, pp. 3052–3057, 1993.

[3] H. Westerhoff *et al.*, "Functional synergism of the magainins PGLa and magainin-2 in Escherichia coli, tumor cells and liposomes," *Eur. J. Biochem.*, vol. 228, no. 2, pp. 257–264, 1995.

[4] V. Chinchar, L. Bryan, U. Silphadaung, E. Noga, D. Wade, and L. Rollins-Smith, "Inactivation of viruses infecting ectothermic animals by amphibian and piscine antimicrobial peptides," *Virology*, vol. 323, no. 2, pp. 268–275, 2004.

[5] L. Rollins-Smith *et al.*, "Antimicrobial peptide defenses against pathogens associated with global amphibian declines," *Dev. Comp. Immunol.*, vol. 26, no. 1, pp. 63–72, 2002.

[6] J. Conlon *et al.*, "Host-defense peptides in skin secretions of the tetraploid frog Silurana epitropicalis with potent activity against methicillin-resistant Staphylococcus aureus (MRSA)," *Peptides*, vol. 37, no. 1, pp. 113–119, 2012.

[7] J. Oscarsson, Y. Mizunoe, L. Li, X. Lai, A. Wieslander, and E. Uhlin, "Molecular analysis of the cytolytic protein ClyA (SheA) from Escherichia coli," *Mol. Microbiol.*, vol. 32, no. 6, pp. 1226–1238, 1999.

[8] A. Atkins *et al.*, "Structure-function relationships of a novel bacterial toxin, Hemolysin E the role of αG," *J. Biol. Chem.*, vol. 275, no. 52, pp. 41150–41155, 2000.

[9] A. Ludwig *et al.*, "Mutations affecting export and activity of cytolysin A from Escherichia coli," *J. Bacteriol.*, vol. 192, no. 15, pp. 4001–4011, 2010.

[10] N. Eifler *et al.*, "Cytotoxin ClyA from Escherichia coli assembles to a 13-meric pore independent of its redox-state," *EMBO J.*, vol. 25, no. 11, pp. 2652–2661, 2006.

[11] W. Hoiles, V. Krishnamurthy, and B. Cornell, "Modelling the bioelectronic interface in engineered tethered membranes: From biosensing to electroporation," *IEEE Trans. Biomed. Circuits Syst.*, vol. 9, no. 3, pp. 321–333, Jun. 2014.

[12] H. Wang, A. Thiele, and L. Pilon, "Simulations of cyclic voltammetry for electric double layers in asymmetric electrolytes: A generalized modified Poisson-Nernst-Planck model," *J. Phys. Chem. C*, vol. 117, no. 36, pp. 18286–18297, 2013.

[13] T. Husslein, D. Newns, P. Pattnaik, Q. Zhong, P. Moore, and M. Klein, "Constant pressure and temperature molecular-dynamics simulation of the hydrated diphytanolphosphatidylcholine lipid bilayer," *J. Chem. Phys.*, vol. 109, no. 7, pp. 2826–2832, 1998.

[14] W. Shinoda, M. Mikami, T. Baba, and M. Hato, "Dynamics of a highly branched lipid bilayer: A molecular dynamics study," *Chem. Phys. Lett.*, vol. 390, no. 1, pp. 35–40, 2004.

[15] S. Tristram-Nagle *et al.*, "Structure and water permeability of fully hydrated diphytanoyIPC," *Chem. Phys. Lipids*, vol. 163, no. 6, pp. 630–637, 2010.

[16] P. Bressloff and J. Newby, "Stochastic models of intracellular transport," *Rev. Mod. Phys.*, vol. 85, pp. 135–196, 2013.

[17] F. Heinrich *et al.*, "A new lipid anchor for sparsely tethered bilayer lipid membranes," *Langmuir*, vol. 25, no. 7, pp. 4219–4229, 2009.

[18] W. Hoiles, V. Krishnamurthy, C. Cranfield, and B. Cornell, "An engineered membrane to measure electroporation: Effect of tethers and bioelectronic interface," *Biophys. J.*, vol. 107, no. 6, pp. 1339–1351, 2014.

[19] Z. Hughes and T. Walsh, "Structure of the electrical double layer at aqueous gold and silver interfaces for saline solutions," *J. Colloid Interface Sci.*, vol. 436, pp. 99–110, 2014.

[20] J. Brody, P. Yager, R. Goldstein, and R. Austin, "Biotechnology at low Reynolds numbers," *Biophys. J.*, vol. 71, no. 6, pp. 3430–3441, 1996.

[21] P. Smadbeck and Y. Kaznessis, "Stochastic model reduction using a modified Hill-type kinetic rate law," *J. Chem. Phys.*, vol. 137, no. 23, p. 234109, 2012.

[22] J. Thompson, B. Cronin, H. Bayley, and M. Wallace, "Rapid assembly of a multimeric membrane protein pore," *Biophys. J.*, vol. 101, no. 11, pp. 2679–2683, 2011.

[23] S. Vaidyanathan, P. Sathyanarayana, P. Maiti, S. Visweswariah, and K. Ayappa, "Lysis dynamics and membrane oligomerization pathways for Cytolysin A (ClyA) pore-forming toxin," *RSC Adv.*, vol. 4, pp. 4930–4942, 2014.

[24] A. Cirac *et al.*, "The molecular basis for antimicrobial activity of pore-forming cyclic peptides," *Biophys. J.*, vol. 100, no. 10, pp. 2422–2431, 2011.

[25] C. Cruickshank, R. Minchin, A. Dain, and B. Martinac, "Estimation of the pore size of the large-conductance mechanosensitive ion channel of Escherichia coli," *Biophys. J.*, vol. 73, no. 4, pp. 1925–1931, 1997.

[26] S. Marrink, H. Risselada, S. Yefimov, D. Tieleman, and A. Vries, "The MARTINI force field: Coarse grained model for biomolecular simulations," *J. Phys. Chem. B*, vol. 111, no. 27, pp. 7812–7824, 2007.

[27] L. Monticelli, S. Kandasamy, X. Periole, R. Larson, P. Tieleman, and S. Marrink, "The MARTINI coarse-grained force field: Extension to proteins," *J. Chem. Theory Comput.*, vol. 4, no. 5, pp. 819–834, 2008.

[28] X. Periole and S. Marrink, "The MARTINI coarse-grained force field," in *Biomolecular Simulations*, New York, NY, USA: Springer, vol. 924, 2012.

[29] J. Lim and J. Klauda, "Lipid chain branching at the iso-and anteiso-positions in complex Chlamydia membranes: A molecular dynamics study," *Biochim. Biophys. Acta (BBA) Biomembr.*, vol. 1808, no. 1, pp. 323–331, 2011.

[30] K. Shinoda, W. Shinoda, and M. Mikami, "Molecular dynamics simulation of an archaeal lipid bilayer with sodium chloride," *Phys. Chem. Chem. Phys.*, vol. 9, no. 5, pp. 643–650, 2007.

[31] W. Shinoda, M. Mikami, T. Baba, and M. Hato, "Molecular dynamics study on the effect of chain branching on the physical properties of lipid bilayers: Structural stability," *J. Phys. Chem. B*, vol. 107, no. 50, pp. 14030–14035, 2003.

[32] K. Shinoda, W. Shinoda, T. Baba, and M. Mikami, "Comparative molecular dynamics study of ether-and ester-linked phospholipid bilayers," *J. Chem. Phys.*, vol. 121, no. 19, pp. 9648–9654, 2004.

[33] R. Karjiban, N. Shaari, U. Gunasakaran, and M. Basri, "A coarse-grained molecular dynamics study of DLPC, DMPC, DPPC, and DSPC mixtures in aqueous solution," *J. Chem.*, vol. 2013, pp. 1–6, 2013.

[34] S. Yesylevskyy, L. Schäfer, D. Sengupta, and S. Marrink, "Polarizable water model for the coarse-grained MARTINI force field," *PLoS Comput. Biol.*, vol. 6, no. 6, p. e1000810, 2010.

[35] S. Wang and R. Larson, "Water channel formation and ion transport in linear and branched lipid bilayers," *Phys. Chem. Chem. Phys.*, vol. 16, no. 16, pp. 7251–7262, 2014.

[36] J. Ulmschneider, J. Smith, M. Ulmschneider, A. Ulrich, and E. Strandberg, "Reorientation and dimerization of the membrane-bound antimicrobial peptide PGLa from microsecond all-atom MD simulations," *Biophys. J.*, vol. 103, no. 3, pp. 472–482, 2012.

[37] T. Wieprecht, O. Apostolov, M. Beyermann, and J. Seelig, "Membrane binding and pore formation of the antibacterial peptide PGLa: Thermodynamic and mechanistic aspects," *Biochemistry*, vol. 39, no. 2, pp. 442–452, 2000.

[38] E. Strandberg, P. Wadhwani, P. Tremouilhac, U. Dürr, and A. Ulrich, "Solid-state NMR analysis of the PGLa peptide orientation in DMPC bilayers: Structural fidelity of 2H-labels versus high sensitivity of 19F-NMR," *Biophys. J.*, vol. 90, no. 5, pp. 1676–1686, 2006.

[39] B. Bechinger, M. Zasloff, and S. Opella, "Structure and dynamics of the antibiotic peptide PGLa in membranes by solution and solid-state nuclear magnetic resonance spectroscopy," *Biophys. J.*, vol. 74, no. 2, pp. 981–987, 1998.
[40] E. Strandberg, P. Tremouilhac, P. Wadhwani, and A. Ulrich, "Synergistic transmembrane insertion of the heterodimeric PGLa/magainin 2 complex studied by solid-state NMR," *Biochim. Biophys. Acta (BBA) Biomembr.*, vol. 1788, no. 8, pp. 1667–1679, 2009.
[41] R. Glaser, C. Sachse, U. Dürr, P. Wadhwani, and A. Ulrich, "Orientation of the antimicrobial peptide PGLa in lipid membranes determined from ^{19}F-NMR dipolar couplings of 4-CF3-phenylglycine labels," *J. Magn. Reson.*, vol. 168, no. 1, pp. 153–163, 2004.
[42] P. Tremouilhac, E. Strandberg, P. Wadhwani, and A. Ulrich, "Synergistic transmembrane alignment of the antimicrobial heterodimer PGLa/magainin," *J. Biol. Chem.*, vol. 281, no. 43, pp. 32089–32094, 2006.
[43] S. Afonin, S. Grage, M. Ieronimo, P. Wadhwani, and A. Ulrich, "Temperature-dependent transmembrane insertion of the amphiphilic peptide PGLa in lipid bilayers observed by solid state F-NMR spectroscopy," *J. Amer. Chem. Soc.*, vol. 130, no. 49, pp. 16512–16514, 2008.
[44] E. Strandberg, P. Tremouilhac, P. Wadhwani, and A. Ulrich, "Synergistic transmembrane insertion of the heterodimeric PGLa/magainin 2 complex studied by solid-state NMR," *Biochim. Biophys. Acta (BBA) Biomembr.*, vol. 1788, no. 8, pp. 1667–1679, 2009.
[45] L. Thøgersen, B. Schiøtt, T. Vosegaard, N. Nielsen, and E. Tajkhorshid, "Peptide aggregation and pore formation in a lipid bilayer: A combined coarse-grained and all atom molecular dynamics study," *Biophys. J.*, vol. 95, no. 9, pp. 4337–4347, 2008.
[46] H. Woo and A. Wallqvist, "Spontaneous buckling of lipid bilayer and vesicle budding induced by antimicrobial peptide magainin 2: A coarse-grained simulation study," *J. Phys. Chem. B*, vol. 115, no. 25, pp. 8122–8129, 2011.
[47] K. Santo and M. Berkowitz, "Difference between magainin-2 and melittin assemblies in phosphatidylcholine bilayers: Results from coarse-grained simulations," *J. Phys. Chem. B*, vol. 116, no. 9, pp. 3021–3030, 2012.
[48] A. Chetwynd, C. Wee, B. Hall, and M. Sansom, "The energetics of transmembrane helix insertion into a lipid bilayer," *Biophys. J.*, vol. 99, no. 8, pp. 2534–2540, 2010.
[49] W. Humphrey, A. Dalke, and K. Schulten, "VMD—Visual molecular dynamics," *J. Mol. Graph.*, vol. 14, no. 1, pp. 33–38, 1996.
[50] R. Pastor and M. Karplus, "Parametrization of the friction constant for stochastic simulations of polymers," *J. Phys. Chem.*, vol. 92, no. 9, pp. 2636–2641, 1988.
[51] J. Knight, M. Lerner, J. Marcano-Velázquez, R. Pastor, and J. Falke, "Single molecule diffusion of membrane-bound proteins: Window into lipid contacts and bilayer dynamics," *Biophys. J.*, vol. 99, no. 9, pp. 2879–2887, 2010.
[52] R. Mills, "Self-diffusion in normal and heavy water in the range 1-45. degrees," *J. Phys. Chem.*, vol. 77, no. 5, pp. 685–688, 1973.
[53] E. Salnikov and B. Bechinger, "Lipid-controlled peptide topology and interactions in bilayers: Structural insights into the synergistic enhancement of the antimicrobial activities of PGLa and magainin 2," *Biophys. J.*, vol. 100, no. 6, pp. 1473–1480, 2011.
[54] R. Glaser *et al.*, "Concentration-dependent realignment of the antimicrobial peptide PGLa in lipid membranes observed by solid-state ^{19}F-NMR," *Biophys. J.*, vol. 88, no. 5, pp. 3392–3397, 2005.
[55] E. Strandberg, P. Wadhwani, P. Tremouilhac, U. Dürr, and A. Ulrich, "Solid-state NMR analysis of the PGLa peptide orientation in DMPC bilayers: Structural fidelity of ^{2}H-labels versus high sensitivity of ^{19}F-NMR," *Biophys. J.*, vol. 90, no. 5, pp. 1676–1686, 2006.
[56] G. Valincius, T. Meskauskas, and F. Ivanauskas, "Electrochemical impedance spectroscopy of tethered bilayer membranes," *Langmuir*, vol. 28, no. 1, pp. 977–990, 2011.
[57] C. Cranfield *et al.*, "Transient potential gradients and impedance measures of tethered bilayer lipid membranes: Pore-forming peptide insertion and the effect of electroporation," *Biophys. J.*, vol. 106, no. 1, pp. 182–189, 2014.
[58] C. Chang and J. Meienhofer, "Solid-phase peptide synthesis using mild base cleavage of N-α-Fluorenylmethyloxycarbonylamino acids, exemplified by a synthesis of dihydrosomatostatin," *Int. J. Peptide Protein Res.*, vol. 11, no. 3, pp. 246–249, 1978.
[59] G. Fields and R. Noble, "Solid phase peptide synthesis utilizing 9-fluorenylmethoxycarbonyl amino acids," *Int. J. Peptide Protein Res.*, vol. 35, no. 3, pp. 161–214, 1990.
[60] S. Afonin *et al.*, "4-Fluorophenylglycine as a label for 19F NMR structure analysis of membrane-associated peptides," *ChemBioChem*, vol. 4, no. 11, pp. 1151–1163, 2003.
[61] P. Amestoy, I. Duff, J. L'Excellent, and J. Koster, "A fully asynchronous multifrontal solver using distributed dynamic scheduling," *SIAM J. Matrix Anal. Appl.*, vol. 23, no. 1, pp. 15–41, 2001.
[62] P. Brown, A. Hindmarsh, and L. Petzold, "Using Krylov methods in the solution of large-scale differential-algebraic systems," *SIAM J. Sci. Comput.*, vol. 15, no. 6, pp. 1467–1488, 1994.
[63] H. Fischer, I. Polikarpov, and A. Craievich, "Average protein density is a molecular-weight-dependent function," *Protein Sci.*, vol. 13, no. 10, pp. 2825–2828, 2004.
[64] H. Berendsen, D. Spoel, and R. Drunen, "GROMACS: A message-passing parallel molecular dynamics implementation," *Comput. Phys. Commun.*, vol. 91, nos. 1–3, pp. 43–56, 1995.
[65] D. Spoel, E. Lindahl, B. Hess, G. Groenhof, A. Mark, and H. Berendsen, "GROMACS: Fast, flexible and free," *J. Comput. Chem.*, vol. 26, pp. 1701–1718, 2005.
[66] B. Hess, C. Kutzner, D. Spoel, and E. Lindahl, "GROMACS 4: Algorithms for highly efficient, load-balanced, and scalable molecular simulation," *J. Chem. Theory Comput.*, vol. 4, no. 3, pp. 435–447, 2008.
[67] H. Berendsen, J. Postma, A. D. W. Gunsteren, and J. Haak, "Molecular dynamics with coupling to an external bath," *J. Chem. Phys.*, vol. 81, no. 8, pp. 3684–3690, 1984.
[68] H. Leontiadou, A. Mark, and S. Marrink, "Molecular dynamics simulations of hydrophilic pores in lipid bilayers," *Biophys. J.*, vol. 86, no. 4, pp. 2156–2164, 2004.
[69] J. Goose and M. Sansom, "Reduced lateral mobility of lipids and proteins in crowded membranes," *PLoS Comput. Biol.*, vol. 9, no. 4, p. e1003033, 2013.
[70] R. Waheed, Q. Tjärnhammar, and O. Edholm, "Phase transitions in coarse-grained lipid bilayers containing cholesterol by molecular dynamics simulations," *Biophys. J.*, vol. 103, no. 10, pp. 2125–2133, 2012.

William Hoiles received the M.A.Sc. degree from the Department of Engineering Science, Simon Fraser University, Burnaby, Canada, in 2012, and the Ph.D. degree in electrical and computer engineering from the University of British Columbia, Vancouver, BC, Canada, in 2015. He is currently a Postdoctoral Researcher in electrical and computer engineering with the University of British Columbia. His research interests include the bioelectronic interface and social sensors.

Vikram Krishnamurthy (S'90–M'91–SM'99–F'05) received the bachelor's degree from the University of Auckland, Auckland, New Zealand, in 1988, and the Ph.D. degree from the Australian National University, Canberra, A.C.T., Australia, in 1992. He is currently a Professor and holds the Canada Research Chair with the Department of Electrical Engineering, University of British Columbia, Vancouver, BC, Canada. His research interests include statistical signal processing, computational game theory and stochastic control in social networks. He served as a Distinguished Lecturer for the IEEE Signal Processing Society and an Editor-in-Chief of the IEEE JOURNAL SELECTED TOPICS IN SIGNAL PROCESSING. He was the recipient of an Honorary Doctorate from KTH (Royal Institute of Technology), Stockholm, Sweden, in 2013.